International Journal of Precision Engineering and Manufacturing (2021) 22:287–300
https://doi.org/10.1007/s12541-020-00435-4

Online ISSN 2005-4602
Print ISSN 2234-7593

REGULAR PAPER

Structural Design and Optimization of the Crossbeam of a Computer Numerical Controlled Milling-Machine Tool Using Sensitivity Theory and NSGA-II Algorithm

Xueguang Li[1] · Chongqing Li[1] · Penghui Li[1] · Huizhong Hu[1] · Xiansheng Sui[1]

Received: 16 July 2020 / Revised: 9 October 2020 / Accepted: 26 October 2020 / Published online: 20 January 2021

Abstract
The crossbeam plays a vital role in computer numerical controlled milling machines, especially in machines with a gantry structure, as it directly influences the machining precision. In this study, a machine tool crossbeam was designed, and the modal frequency of the crossbeam was analyzed using the finite element model (FEM) analysis. In the improved structure obtained through FEM analysis, the X-type structure of the internal unit of the crossbeam was replaced by an O-type structure. The specific structure dimensions were further optimized using a neural-network algorithm and a nondominated sorting genetic algorithm. Finally, we calculated the effect of each crossbeam dimension on the mass, deformation, and frequency in a sensitivity analysis. After optimizing the crossbeam dimensions with respect to deformation, modal frequency, and mass, the structural characteristics of the original and optimized crossbeams were compared. After optimization, the mass and deformation were reduced by 7.45% and 3.08%, respectively, and the modal frequency was increased by 0.42%. These results confirm that the optimization improved the performance of the crossbeam structure.

Keywords Finite element models · Sensitivity theory · Neural network · Structure optimization · NSGA-II algorithm

1 Introduction

Finite element modeling is a powerful and efficient method for analyzing part dynamics [1–3]. The continuous development of technology and demand for lightweight design has elevated the role of multi-objective optimization methods [4–6] and modal analysis methods [7] in practical applications. Both types of methods can optimize the test process, reduce the processing time, and reduce the test costs [8–13]. Meanwhile, computer numerical controlled (CNC) machine tools are gaining prominence as they meet the production requirements of geometric accuracy and surface processing quality of machine parts. The capability of a machine tool is assessed by its machining accuracy, and optimizing the structure and specific dimensions can enhance the basic performance of a machine tool.

✉ Xueguang Li
lixueguang@cust.edu.cn

[1] School of Mechanical and Electrical Engineering, Changchun University of Science and Technology, No. 7089, Weixing Road, Changchun, 130022 Jilin Province, P.R. China

Cheng et al. [14] proposed a sensitivity analysis for optimizing the basic parameters of machine tools and demonstrated it on a three-axis machine tool. Ghasemian et al. [15] designed the variables of an optimized organic Rankine cycle using a nondominated sorting genetic algorithm (NSGA-II). Guo et al. [16] performed a sensitivity analysis of geometric errors on a five-axis machine tool and accuracy optimum values are obtained by multi-objective optimization. Khodaygan [17] proposed a novel interactive framework for a computer-aided multi-objective optimization of tolerance design, which allocates the optimal process tolerances of components. This framework simultaneously optimizes the process capability function and overall manufacturing cost. Lin [18] also optimized the tolerance design using a multi-objective optimization method. A network combined with a genetic algorithm can simultaneously optimize the parameters of a high-speed machine tool, which can then be refined in a sensitivity analysis. High-precision machining can meet the tight tolerances imposed on complex mechanical parts. The machine tool is a complex system that must simultaneously move along three prismatic axes [19]. Therefore, its key parts must be properly designed and optimized. The

neural network model structure that best accelerates the design process and improves the optimization and rationality of the design can be found by objective optimization methods such as structural and system optimization. In some grinding machines, the structure optimization must be supplemented via thermodynamic analysis to improve the thermal performance [20]. Tian et al. [21] proposed a multiobjective optimization of process parameters based on the NSGA-II algorithm. The multi-objective optimization of products is increasingly being emphasized for green manufacturing. Tarek et al. [22] proposed a gray rational analysis based on the Taguchi method, which finds the best neural-network model architecture for multiobjective optimization. Ma et al. [23] optimized the parameters of a high-speed spindle system using a genetic algorithm and particle swarm optimization. Xie et al. [24] obtained the Pareto frontier solutions by employing an improved NSGA-II algorithm. In a gray relational analysis, they also optimized the variable blank holder force loading trajectory.

Wang et al. [25] proposed a novel integrated framework for the design and optimization of a machine tool structure. By combining knowledge-based design and multi-stage optimization with integrated computer-aided design and computer-aided engineering, their framework significantly improves the quality and efficiency of the machine-tool design. Xu and Cao [26] proposed an approach to improve the energy efficiency of the production process through scheduling the maintenance actions of the machine tool, taking into account productivity, product quality, and energy consumption.

Shen et al. [27] proposed a new structural dynamic design optimization method for the holistic machine tool. The inner stiffener layout of the machine structure was designed using the Adaptive Growth Method, and the optimization of the machine tool using dynamic sensitivity analysis was studied. Liu et al. [28] studied the lightweight design of the gantry machine tool using twice optimization design method, which integrates zero-order optimization, parameter rounding, and structural re-optimization. The experiments showed that the mass of the whole gantry frame was reduced by 9.24% before and after the optimization. Feng et al. [29] introduced the sustainability performance of machine tools and design optimization of components such as lightweight using topology and bionic methods, structure design with modular design. Baptista et al. [30] presented a new Lean Design-for-X (LDfX) approach embracing the principles of Lean Product Development and Modular Design, for systematic applicability by design engineers and applied it in a real design study of a machine tool. Yuksel et al. [31] demonstrated a hybrid approach that combines the computational contact problem framework and an obtained stable contact stiffness function. In this research, the existing and the proposed methods for contact are investigated utilizing the solid isotropic material with a penalization model (SIMP) algorithm for topology optimization.

The present paper optimizes the structure design of the crossbeam in a CNC milling-machine tool. The framework combines finite element analysis with multi-objective optimization and optimizes the structure and dimensions of the crossbeam using sensitivity theory and a neural-network algorithm.

In this paper, the optimization of the crossbeam in two periods was accomplished. The first time about optimization aims to change the internal structure from X-type to O-type. The consistency of deformation is dependent on the regular shape of the rib. The second time about optimization aims to optimize the dimensions of the crucial ribs using sensitivity theory, adaptive response surface methodology, the BP neural network, and NSGA-II algorithm. After the optimization in two times, the crossbeam is improved from the internal structure to crucial dimensions.

2 Structure Design and Improvement of the Machine Crossbeam

The designed machine is a small CNC milling-machine tool with dimensions of 550 mm × 520 mm × 520 mm. The maximum spindle speed is 24,000 rpm, and the effective machining distances in the [length], [breadth] and [height] directions are 200, 160, and 100 mm, respectively.

The material is needed to be set before making a FEM analysis. Table 1 indicates the material parameters for the machine. The crossbeam and column are fabricated from gray cast iron (HT250) with a density of 7340 kg/m^3, a Young's modulus of 1.3×10^{11} Pa, a Poisson ratio of 0.25, the slide guide is fabricated from GCr15, the base of the machine is marble, and other parts used S45C.

While analyzing the whole machine or part using FEM, the characteristic details have not profound influence on the analysis results but increase the analyzing difficulty and solution time. However, it tends to make the finite element mesh more dense and extend the analyzing time, even it tends to cause errors. Hence, for some tiny or unimportant characteristics which have less influence on part analysis, the simplified model is necessary. For the machine with a

Table 1 Material set for FEM

Materials	Density (kg/m^3)	Young's modulus (Pa)	Poisson's ratio
HT250	7340	1.3×10^{11}	0.25
GCr15	7830	2.19×10^{11}	0.3
S45C	7800	2.1×10^{11}	0.3
Marble	2600	5.5×10^{10}	0.3

gantry structure, the force applied on the cross-beam not only includes cutting force come from the cutting tool, but also includes the weight of the X-axis and Z axis feed system and spindle. The cross beam plays a vital role in machining precision. In this investigation, the machine and parts were modeled and simplified first. Then we set the material parameters and properties. The elements were meshed further. The finite element grid of the beam is quadrilateral, and the number of cells is 147,230. The constraints was applied on the two ends of the cross-beam, with the resultant force of cutting force, weight of X, Z axis applied on the crossbeam. The statics and modal analysis were accomplished. Figure 1 shows the procedure of finite element analysis.

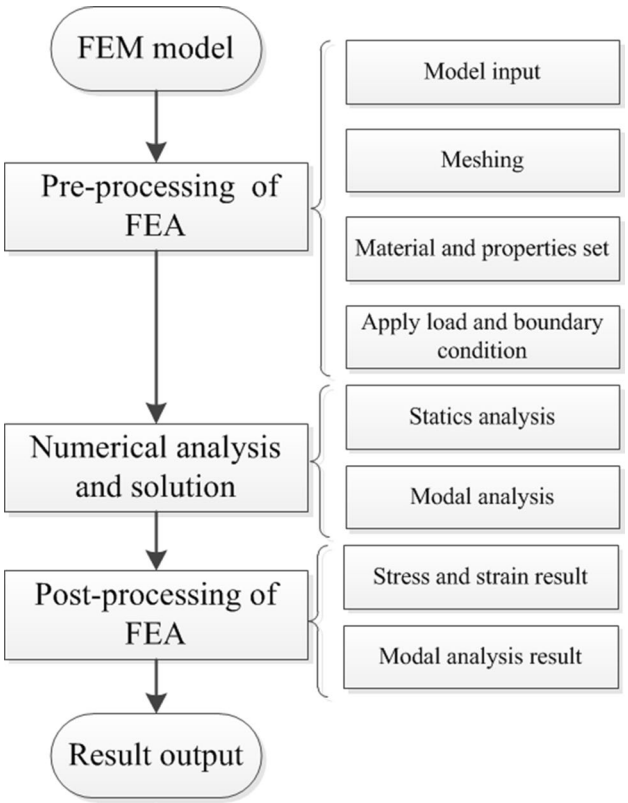

Fig. 1 The procedure of finite element analysis

An X-type structure of its internal elements. The machine and its crossbeam structure are displayed in Fig. 2.

Figure 3 indicates that the biggest deformation occurred in the middle point of the crossbeam, with the value of 0.18574 μm. Besides, the value in the X direction is 0.0318 μm; the value in the Y direction is 0.15101 μm, and the value in the Z direction is 0.0318 μm, 0.108 μm.

As the key part of the whole machine, the crossbeam bears the cutting force and weight of the spindle and feed systems, and plays a vital role in the machining accuracy. It has an impact on the machining precision directly. Therefore, the modal analysis is necessary to investigate whether it creates resonance with the spindle during machining. The modal coordinate will be replaced by a physical coordinate formed by a differential equation of vibration through the modal analysis. After decoupling equations set, the independent equation described by modal coordinate and parameters should be established, so that the system modal parameters can be solved. Hence, the optimization process was preceded by modal analysis. Figure 4 presents the results of the modal analysis.

The first-order modal frequency of the crossbeam was 1604 Hz (Fig. 4a). The higher-order modes with higher frequencies (especially the third-, fifth-, and sixth-order modes) have complex mode shapes or large deformations (Fig. 4b–f). Therefore, the crossbeam structure should be modified further and the spindle speed should be properly selected to avoid resonance, which is probably generated between the spindle motor and cross beam.

Based on the modal analysis results, the internal structure of the crossbeam was optimized as shown in Fig. 4. The internal structure changed from X-type to O-type. The structural differences between these two designs are compared in Fig. 5a.

According to experimental studies, in the internal elements of the beam, the O-type is better than the X-type in terms of static and dynamic characteristics. Changing the internal element structure of the crossbeam from X-shaped to O-shaped reduced the total deformation, equivalent stress, and modal frequency of the crossbeam. Based on analysis, it can be concluded that the O-type structure changed the connection type of the ribs, improved the stress concentration condition in the

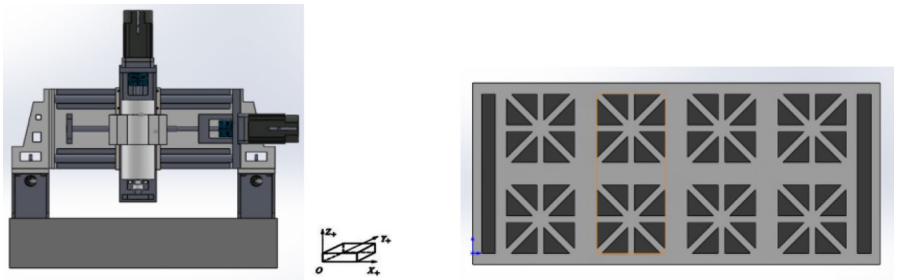

(a) Machine model with a gantry structure **(b)** Structure of crossbeam

Fig. 2 Schematic of the machine and its crossbeam structure. **a** Machine model with a gantry structure. **b** Structure of crossbeam

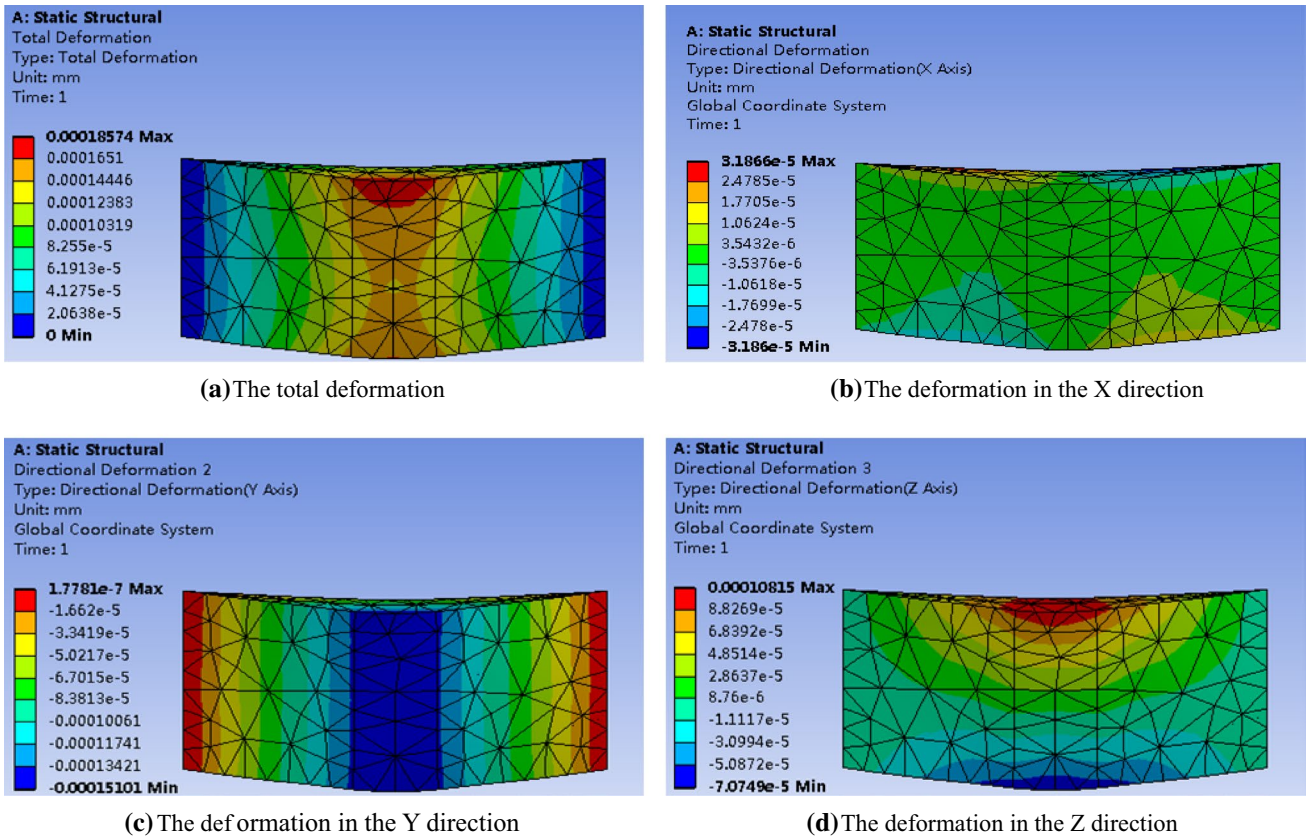

(a) The total deformation

(b) The deformation in the X direction

(c) The def ormation in the Y direction

(d) The deformation in the Z direction

Fig. 3 Statics analysis of the crossbeam. **a** The total deformation. **b** The deformation in the X direction. **c** The deformation in the Y direction. **d** The deformation in the Z direction

center point. The front section of the optimized structure has two slots at each side, providing higher stiffness than the single slot in the original schedule. Table 2 shows the FEM analysis results of both crossbeam designs.

The FEA tool with topology optimization was used to validate the structure designing solution further. Based on the FEM model of the crossbeam, the structure topology optimization was conducted using the variable density method in FEM software. As an efficient method, density is assumed variable. After the discrete of the original structure, taking the unit density as a design variable, the task of structure topology optimization aims to find the inner material distribution of the structure, changing the unit density using algorithm to get the smallest deformation energy.

The mathematical model is shown as follows:

$$\begin{cases} Find\ P = (p_1, p_2, \ldots, p_n) \\ Min\ U = f(P) \\ s.t.\ \ V \le V_0 - V_1 \\ 0 \le P_i \le 1 \ \ (i = 1, 2, \ldots, n) \end{cases}$$

where U is the structure deformation energy, P_i is unit density, V is structure volume, V_0 is structure volume before optimization, V_1 is structure volume of material removal.

Based on the variable density method and topology optimization, the optimum material distribution of the crossbeam is obtained using FEM software, as shown in Fig. 6, the material is gray cast iron (HT250) with a density of 7340 kg/m^3, a Young's modulus of 1.3×10^{11} Pa, a Poisson ratio of 0.25.

The load was applied on the top surface of the crossbeam. Displacement boundary condition was applied on the two sides in vertical direction. The topology and iteration results show that the structure works well and meets the machine structure lightweight demanding.

3 Optimization of the Specific Dimensions

The multi-objective optimized method based on adaptive response surface methodology and NSGA-II algorithm was used for the lightweight design about crossbeam. The deformation, mass and frequency were regarded as

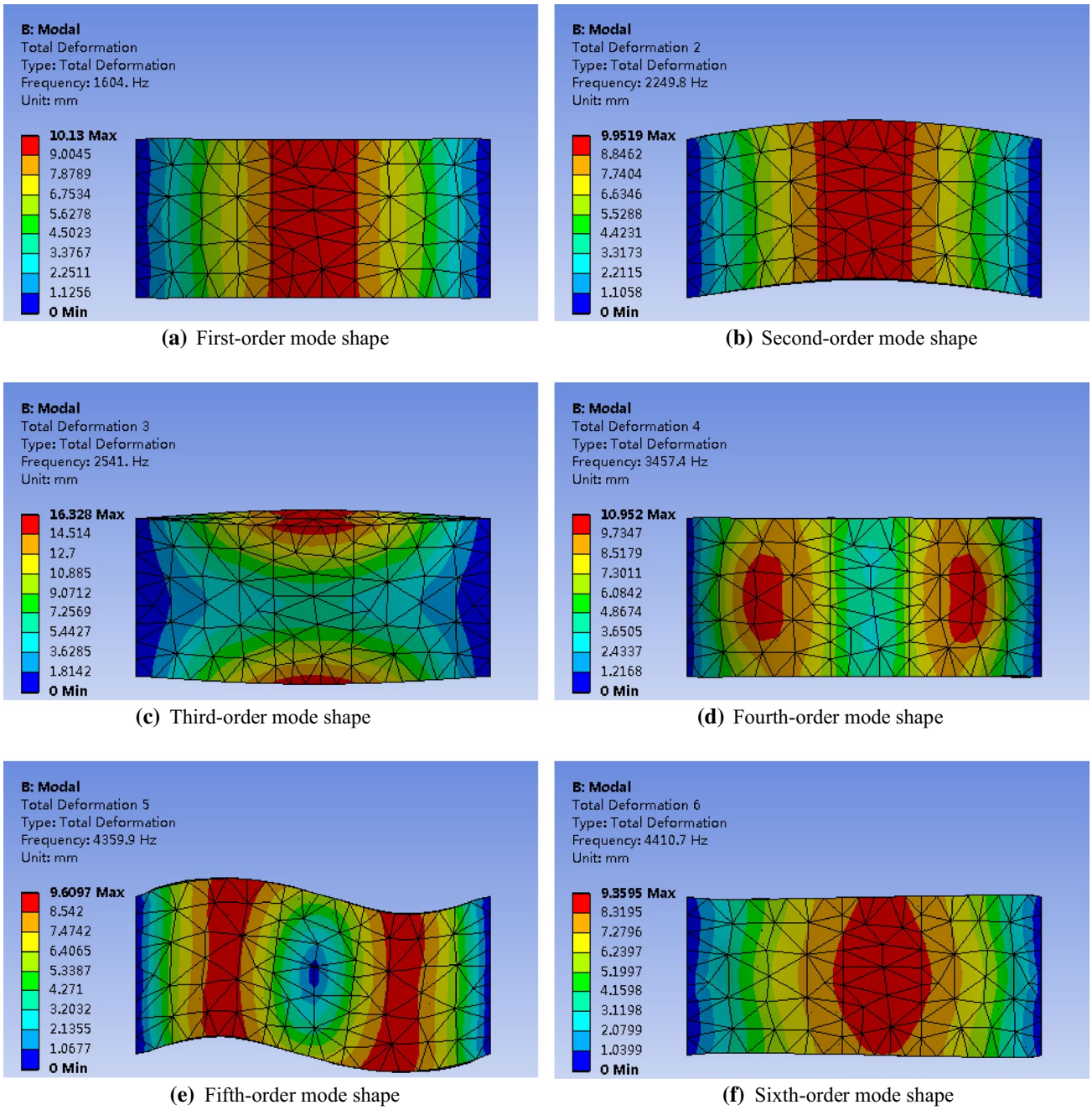

(a) First-order mode shape

(b) Second-order mode shape

(c) Third-order mode shape

(d) Fourth-order mode shape

(e) Fifth-order mode shape

(f) Sixth-order mode shape

Fig. 4 Modal frequencies of the crossbeam. **a** First-order mode shape. **b** Second-order mode shape. **c** Third-order mode shape. **d** Fourth-order mode shape. **e** Fifth-order mode shape. **f** Sixth-order mode shape

optimized function due to the complexity of the crossbeam structure. According to the sensitivity theory, the wall thickness that has different influence on structure sensitivity was balanced, and the important wall thickness dimensions which need to be optimized were filtered. Using adaptive response surface methodology and NSGA-II algorithm, the optimized dimensions were concluded.

3.1 Sensitivity Theory

The structure optimization of the crossbeam performed in this study is based on sensitivity theory. Static deformation sensitivity means that the entire static deformation responds to changes in the design variables:

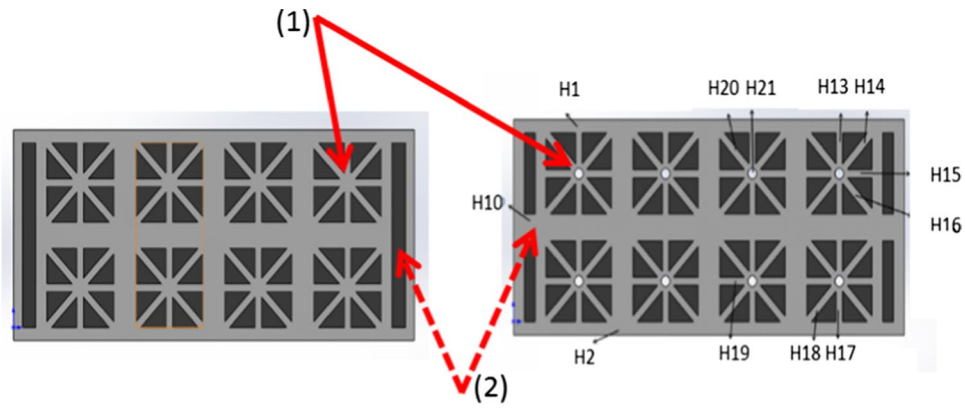

(a) Front sections of the two structures

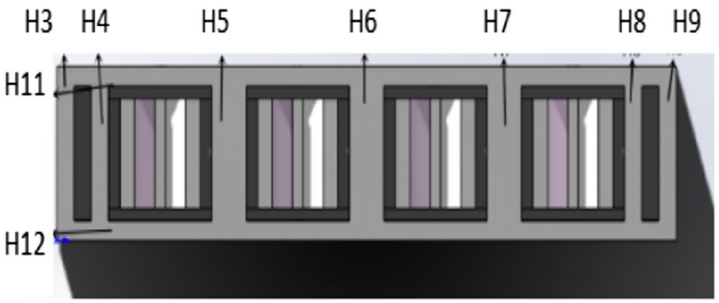

(b) Top–down section of the new crossbeam

Fig. 5 Section of the new crossbeam. The internal elements of the original structure (top left) are changed to O-type (top right). **a** Front sections of the two structures. **b** Top–down section of the new crossbeam

Table 2 Performance comparison of the two crossbeam designs

Parameters	Crossbeam (X-type structure)	Crossbeam (O-type structure)
Total deformation (μm)	0.1857	0.1847
Equivalent stress (MPa)	0.16726	0.14814
Frequency of the first-order modal (Hz)	1604	1610.5
Mass (kg)	21.42	20.534

$$S_{bx}(x_1, x_2 \ldots, x_n) = \frac{\partial b(x_1, x_2 \ldots, x_n)}{\partial x_i}, \tag{1}$$

$$S_{mx}(x_1, x_2 \ldots, x_n) = \frac{\partial m(x_1, x_2 \ldots, x_n)}{\partial x_i}, \tag{2}$$

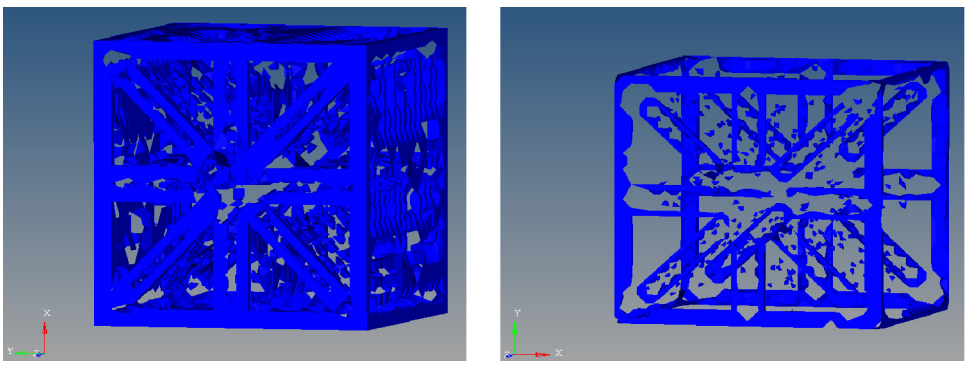

(a) Iteration progress(30%)

(b) Second iteration(80%)

Fig. 6 Material removal of the crossbeam unit based on topology analysis. **a** Iteration progress (30%). **b** Second iteration (80%)

$$S_{bm} = \frac{\partial b(x_1, x_2 \ldots, x_n)}{\partial m(x_1, x_2 \ldots, x_n)} = \frac{\frac{\partial b}{\partial x_i}}{\frac{\partial m}{\partial x_i}} = \frac{S_{bx}}{S_{mx}}, \quad (3)$$

where $(x_1, x_2 \ldots, x_n)$ are the values of the selected dimensions, b is the total deformation of the structure (μm), m is the mass of the structure (kg), S_{bx} and S_{mx} are the sensitivities of the total deformation and mass to changes in the dimensions, respectively, and S_{bm} is the sensitivity of the total deformation to mass changes.

The dynamic sensitivity refers to the frequency sensitivity of the part to changes of the selected dimension variables. It is calculated as follows:

$$M\ddot{X}(t) + KX(t) = 0, \quad (4)$$

where M and K are matrices describing the system mass and stiffness, respectively, and $\ddot{x}$ and x are the n-dimensional acceleration and displacement vectors of the mass nodes, respectively. The displacement vector is given by the following equation:

$$x = A \sin(\omega t), \quad (5)$$

where A is the amplitude (mm) and ω is the vibration frequency of the vector (Hz).

Substituting $\ddot{x}$ *and* x into Eq. (4), we get the characteristic formula:

$$\left(K - \omega_j^2 M\right) A_j = 0, \quad (6)$$

where ω_j and A_j are the jth-order modal frequency and amplitude of the structure, respectively.

Taking the partial derivative of Eq. (6) with respect to the dimension design variable x_i, multiplying on the left by A_j^T, and substituting $\omega = 2\pi f$, the sensitivity of the modal frequency of the structure to a given dimension variable is obtained as follows:

$$S_{fx} = \frac{\partial f(x_1, x_2 \ldots, x_n)}{\partial x_i} = \frac{1}{8\pi^2 f} A_j^T A_j^T \frac{\partial K}{\partial x_i} A_j - \frac{f}{2} \omega_j^2 A_j^T A_j \frac{\partial M}{\partial x_i}, \quad (7)$$

From Eqs. (2) to (7), the sensitivity of the modal frequency to mass is obtained as follows:

$$S_{fm} = \frac{\partial f(x_1, x_2 \ldots, x_n)}{\partial m(x_1, x_2 \ldots, x_n)} = \frac{\frac{\partial f}{\partial x_i}}{\frac{\partial m}{\partial x_i}} = \frac{S_{fx}}{S_{mx}}, \quad (8)$$

Figure 7 is the flow chart of the sensitivity analysis of crossbeam.

3.2 Sample Design

The optimized crossbeam is a box with O-shaped structure units. The outer wall is 8- and 10-mm thick, and the inner wall is 10 mm thick. The outer wall and rib thicknesses of the O-shaped element were selected as the experimental elements for optimization. The aim is to optimize the values of the 21 dimension variables listed in Table 3. Taking the original value

Table 3 Variables in the structure dimension design

Variable number	Original value (mm)	Range (mm)
H1–H4	10	8–12
H5–H7	20	18–22
H8–H9, H12	10	8–12
H10	20	18–22
H11	8	6–10
H13–H20	6	4–8
H21	6	6–10

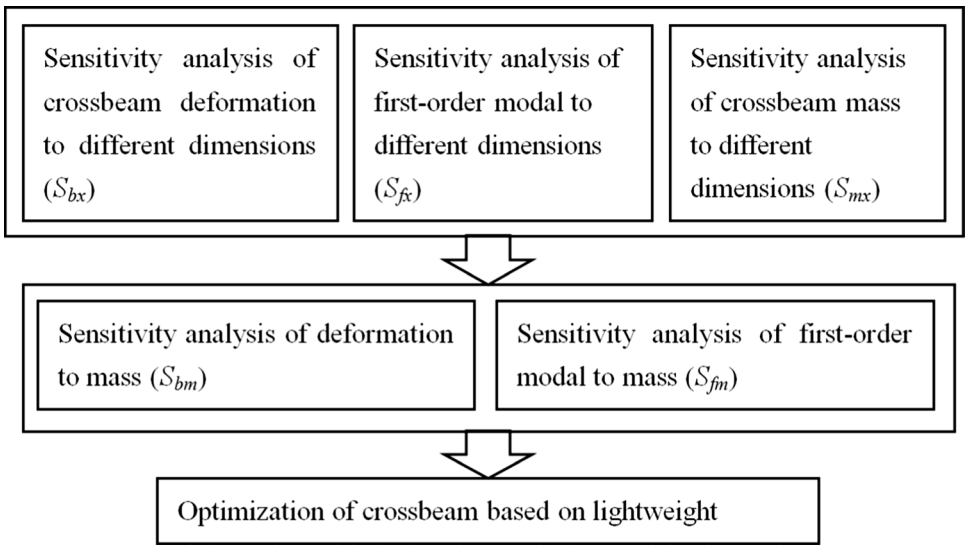

Fig. 7 Flow chart of sensitivity analysis

Table 4 Deformation of crossbeam for different values of each dimension

Dimension number	− 2	− 1	0	1	2
H1	0.19253	0.18849	0.1847	0.18191	0.17788
H2	0.18902	0.18598	0.1847	0.18311	0.18068
H3	0.18538	0.18476	0.1847	0.18446	0.18398
H4	0.18558	0.18526	0.1847	0.18449	0.18413
H5	0.18927	0.18681	0.1847	0.18409	0.18334
H6	0.18669	0.18592	0.1847	0.18377	0.18319
H7	0.1895	0.18692	0.1847	0.18409	0.18328
H8	0.18563	0.18524	0.1847	0.18446	0.18402
H9	0.18538	0.18506	0.1847	0.18449	0.18408
H10	0.18505	0.18497	0.1847	0.18455	0.18437
H11	0.20351	0.19095	0.1847	0.17837	0.16979
H12	0.18585	0.18541	0.1847	0.18442	0.1821
H13	0.18568	0.18534	0.1847	0.18339	0.18263
H14	0.18584	0.18517	0.1847	0.18315	0.18256
H15	0.18626	0.1853	0.1847	0.18384	0.18274
H16	0.18573	0.18533	0.1847	0.18358	0.1824
H17	0.18572	0.18523	0.1847	0.18391	0.18301
H18	0.1858	0.18531	0.1847	0.1839	0.18266
H19	0.18622	0.18556	0.1847	0.18379	0.18254
H20	0.18574	0.18534	0.1847	0.18364	0.1824
H21	0.18103	0.18299	0.1847	0.18601	0.18738

Table 5 First-order modal frequency of the crossbeam for different values of each dimension

Dimension number	− 2	− 1	0	1	2
H1	1603	1607.5	1610.5	1615.4	1617.9
H2	1603	1607.5	1610.5	1615.4	1617.9
H3	1606.9	1607.6	1610.5	1611.8	1614.4
H4	1604.5	1608.6	1610.5	1613.5	1615.4
H5	1604.5	1607.6	1610.5	1610.9	1611.3
H6	1614.8	1613.4	1610.5	1610.1	1609.4
H7	1604.5	1607.6	1610.5	1610.9	1611.3
H8	1604.5	1608.6	1610.5	1613.5	1615.4
H9	1606.9	1607.6	1610.5	1611.8	1614.4
H10	1608	1609.4	1610.5	1613.8	1615.5
H11	1600.3	1604.8	1610.5	1613.8	1616
H12	1600.3	1604.8	1610.5	1613.8	1616
H13	1613.4	1611.2	1610.5	1609.7	1608.2
H14	1606.5	1607.9	1610.5	1611.2	1614.7
H15	1605.6	1608.6	1610.5	1611.9	1614.7
H16	1606.5	1607.9	1610.5	1611.2	1614.7
H17	1613.4	1611.2	1610.5	1609.7	1608.2
H18	1606.5	1607.9	1610.5	1611.2	1614.7
H19	1605.6	1608.6	1610.5	1611.9	1614.7
H20	1606.5	1607.9	1610.5	1611.2	1614.7
H21	1612.9	1611.2	1610.5	1610.4	1610.3

of each variable as the center point, sets of five variables were generated by implementing two increments and two decrements with a step size of 1 mm. For example, the variable set for H1–H4 was generated as {8, 9, 10, 11, 12}. The multi-objective optimized function was designed as follows:

$$\begin{cases} x_i \\ S_f \geq 1610.5\ \text{Hz} \\ S_b \leq 0.1847\ \mu\text{m} \\ m_{min} \end{cases}, \tag{9}$$

where x_i is the wall thickness (designed variable), $S_f \geq 1610.5$ Hz constrains the first-order frequency to at least 1610.5 Hz, and $S_b \leq 0.1847$ µm constrains the entire deformation to at most 0.1847 µm. m_{min} is the objective function that minimizes the mass of the crossbeam.

4 Results and Discussion

4.1 Sensitivity Calculation and Analysis Results

4.1.1 Crossbeam Deformation and First-Order Modal Sensitivity Analysis

The relation between the variable values and crossbeam deformation of the samples prepared in Sect. 3.2 were analyzed through FEM analysis. The results showed almost linear relationships between the crossbeam deformation and the values of each dimension variable and between the first-order modal frequency and the values of each dimension variable (see Tables 4, 5, respectively).

The sensitivities of the deformation to the 21-dimension variables is plotted in Fig. 8. As shown in Fig. 8, the deformation responded most sensitively to the dimension variable H11. Recall that the Z axis and spindle are connected with the crossbeam at the H11 side (Fig. 2). Therefore, the high sensitivity of deformation to the H11 dimension is expected. The modal frequency to the 21-dimension variables is plotted in Fig. 9.

4.1.2 Mass Sensitivity Analysis of Crossbeam

The mass of the crossbeam increased when the value of any selected dimension increased. The crossbeam mass was linearly related to the dimension variables; its sensitivity to each dimension is plotted in Fig. 10.

Because H11 dominated in all three sensitivity profiles, we must determine whether it has a significant impact on the constraints. As shown in Fig. 11. The deformation exhibits linear change while changing the dimension from 6 to 10 mm. It shows that the total

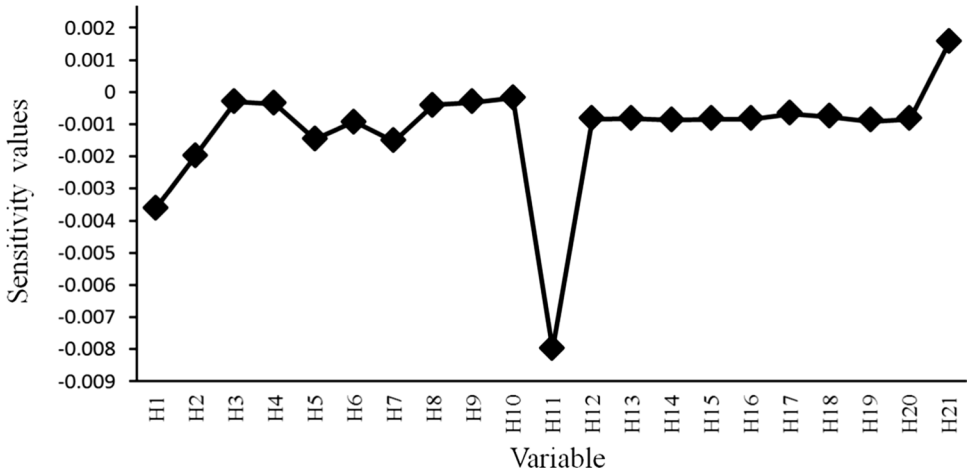

Fig. 8 Sensitivity of deformation to each dimension variable

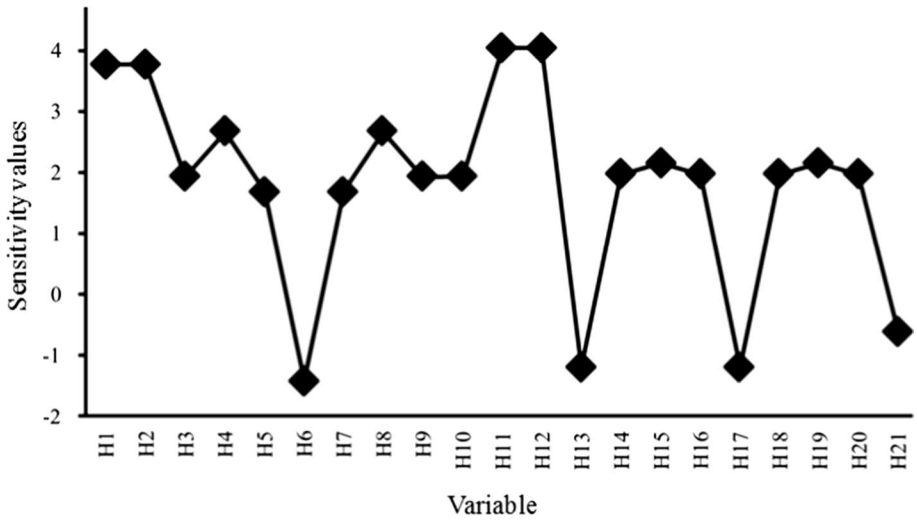

Fig. 9 Sensitivity of first-order modal frequency to each dimension variable

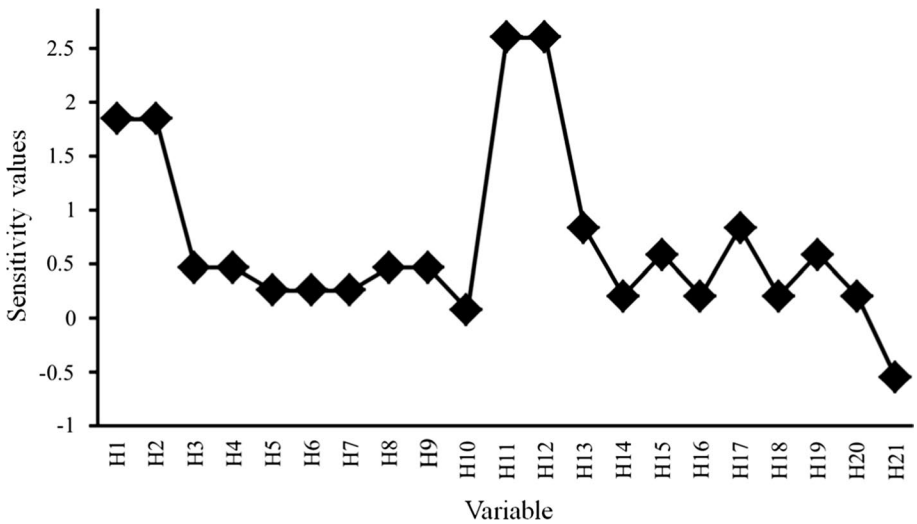

Fig. 10 Sensitivity of cross-beam mass to each dimension variable

deformation decreased with the increase of the dimension. Moreover, the frequency and mass increased while the dimension increased. Therefore, it can be concluded that the influence of H11 on the total deformation, first-order modal frequency and mass were consistent with the actual situation.

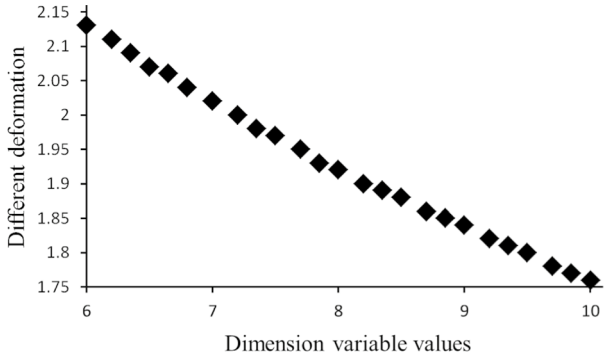

(a) The influence trend of H11 to total deformation

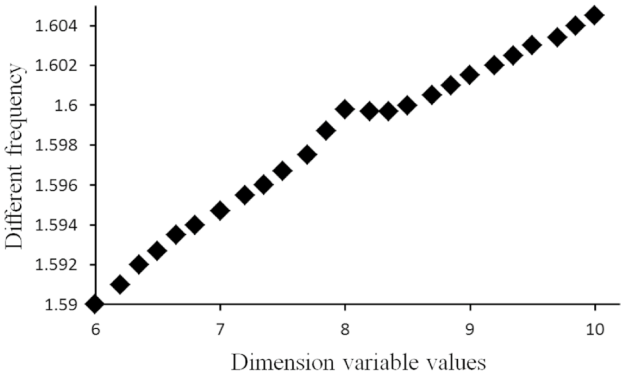

(b) The influence trend of H11 to first-order modal frequency

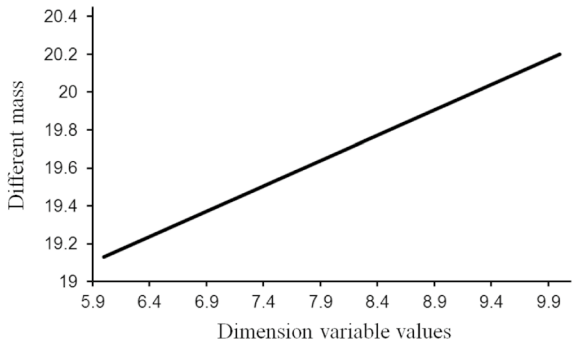

(c) The influence trend of H11 to mass

Fig. 11 The influence trend of dimension H11 to deformation, frequency, and mass. **a** The influence trend of H11 to total deformation. **b** The influence trend of H11 to first-order modal frequency. **c** The influence trend of H11 to mass

4.2 Optimization of the Specific Dimension Variables

Based on sensitivity theory and adaptive response surface methodology, the relation between dimension and mass, the sensitivities of the crossbeam deformation and modal frequency to the mass increment were analyzed and calculated indirectly; the results are given in Table 6.

Table 6 Sensitivities of crossbeam deformation and first-order frequency to mass increment

Dimension number	Sensitivity of deformation to mass increment	Sensitivity of frequency to mass increment
H1	− 0.00195	2.046133
H2	− 0.00106	2.046133
H3	− 0.00067	4.129032
H4	− 0.00079	5.741935
H5	− 0.00572	6.627451
H6	− 0.00359	− 5.52941
H7	− 0.00599	6.627451
H8	− 0.00086	5.741935
H9	− 0.00068	4.129032
H10	− 0.00223	24.25
H11	− 0.00308	1.555342
H12	− 0.00033	1.555342
H13	− 0.00097	− 1.42943
H14	− 0.00409	9.380952
H15	− 0.00144	3.644068
H16	− 0.004	9.380952
H17	− 0.00081	− 1.42943
H18	− 0.00366	9.380952
H19	− 0.00155	3.644068
H20	− 0.00399	9.380952
H21	− 0.00285	1.085973

As shown in Table 6, the dimension variables H5, H6, H7, H14, H16, H18, and H20 significantly influenced the sensitivity of deformation to the mass increment, whereas H1, H2, H10, H11, H15, H19, and H21 exerted a moderate effect, and H3, H4, H8, H9, H10, H12, H13, and H17 exerted a smaller influence. Meanwhile, the variables H4, H5, H6, H7, H8, H10, H14, H16, H18, and H20 significantly influenced the sensitivity of frequency to the mass increment, followed by H1, H2, H3, H9, H15, and H19. The variables H11, H12, H13, H17, and H21 exerted the smallest influence. The more influential variables were selected for further optimization. The optimization variables H1, H2, H4, H5, H6, H7, H8, H10, H11, H14, H15, H16, H18, H19, and H20, (15 dimensions in total) were renamed as shown in Table 7.

In the multi-objective optimization, D1–D12 and E1–E3 were chosen as the independent variables, and the total deformation, first-order modal frequency and mass were assigned as the constraints and optimization targets. Multi-objective optimization was performed using a back-propagation (BP) neural network and the NSGA-II algorithm. The samples were chosen using the space-filling design method. Fifteen-dimension variables were constructed using this method, and 287 groups of samples were chosen. Among these, 277 groups of data were

Table 7 Dimension variables selected for the multiobjective optimization

Variable number	New variable number	Original value (mm)	Range (mm)
H1	E1	10	8–12
H2	E2	10	8–12
H4	D1	10	8–12
H5	D2	20	18–22
H6	D3	20	18–22
H7	D4	20	18–22
H8	D5	10	8–12
H10	E3	20	18–22
H11	D6	8	6–10
H14	D7	6	4–8
H15	D8	6	4–8
H16	D9	6	4–8
H18	D10	6	4–8
H19	D11	6	4–8
H20	D12	6	4–8

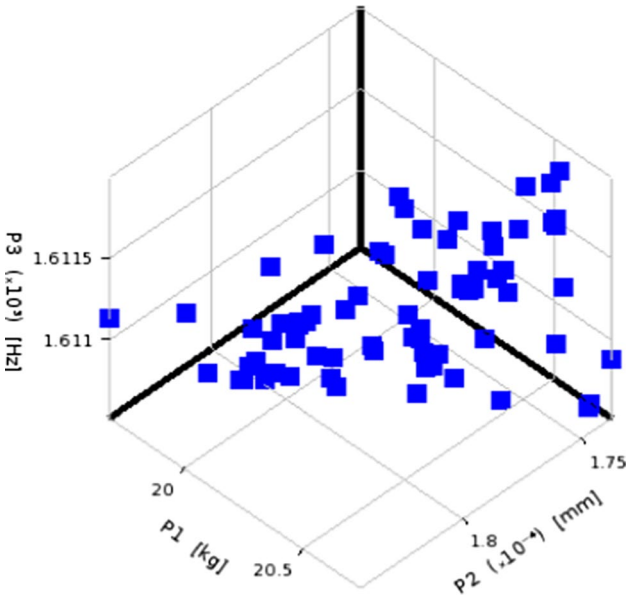

Fig. 13 The values of deformation, frequency, and mass after multi-objective optimization

randomly selected as the training data, and the remaining ten groups were reserved for testing the network.

A three-layer neural network with 15 neural network nodes in the input layer and three neural network nodes in the output layer was constructed. Because there were 19 nodes in the hidden layer (by calculation), the structure of the BP neural network was 15–19–3. The data were normalized, and the learning rate, training error, and the number of training times were set to 0.02, 0.01, and 1000, respectively. Figure 12 shows the relative errors obtained in 10 sets of test data. The maximum prediction errors in the mass, total deformation, and first-order modal frequency were 0.1493%, 1.0586%, and 0.3667%, respectively, which meet the requirements of multi-objective optimization.

The multi-objective optimization of the beam was performed using the NSGA-II algorithm. The relevant parameters in the algorithm were set as follows: number of initial populations = 200, maximum number of evolution iterations = 100, mutation probability = 0.02, crossover probability = 0.98. The Pareto frontier solution is shown in Fig. 13.

The three coordinate axes in Fig. 13 correspond to the total deformation, first-order modal frequency, and mass. The optimum values of the dimension variables are listed in Table 8.

To verify the optimization results, the FEM analysis was repeated using the optimized dimension variables. The parameters of the original and optimized structures are compared in Table 9. The optimization lowered the mass of the crossbeam by 7.45%, reduced the deformation by 3.08%, and increased the modal frequency by 0.42%.

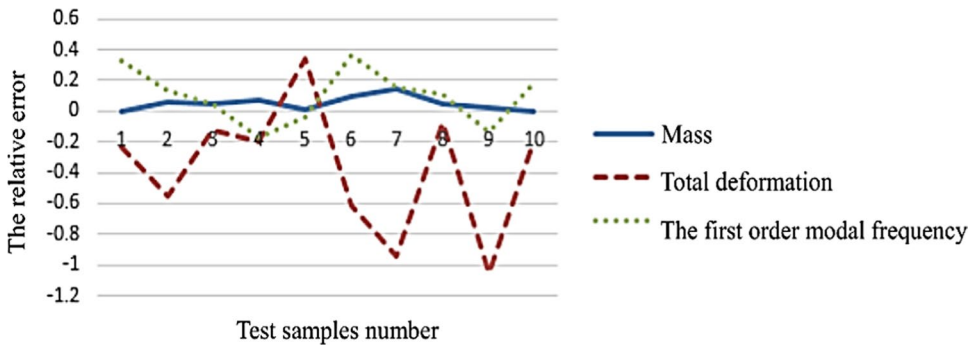

Fig. 12 Error analysis of samples about mass, deformation, and frequency

Table 9 Parameter comparison of the original and optimized crossbeam structures

Parameters	Original structure	Structure with optimum dimensions	Change ratio (%)
Mass (kg)	21.42	19.825	− 7.45
Total deformation (μm)	0.1857	0.17999	− 3.08
Modal frequency (Hz)	1604	1610.7	0.42

Table 8 Optimum value of each variable

Variable	Value	Variable	Value	Variable	Value
D1	11.1	D7	5.6	D11	6.6
D2	18.7	D8	6.1	D12	4.5
D3	18.2	D9	4.1	E1	8.2
D4	19.1	D10	5.3	E2	8
D5	11.7	D6	9.9	E3	11.2

5 Conclusions

Using FEM analysis, this paper performed a modal frequency analysis of a CNC machine crossbeam with an X-type unit structure. The internal structure of the crossbeam was improved by changing the X-type units to O-type units. The characteristic dimensions of the crossbeam were divided into different groups, and their influences on the crossbeam mass, frequency, and deformation were calculated and analyzed using sensitivity theory. From the sensitivity analysis results, 15 dimensions were defined as independent variables using multi-objective optimization. The deformation, modal frequency, and crossbeam mass were input as the constraints and optimization goals into the multi-objective optimization process, comprised of a BP neural network and NSGA-II algorithm. The crossbeam mass decreased by 7.45%. The total deformation of the crossbeam decreased by 3.08%, and the modal frequency of the crossbeam increased by 0.42%. The crossbeam with the optimized structure and dimensions was more lightweight, less deformable, and vibrated at a higher modal frequency than the original design.

Acknowledgements This work was supported by the Jilin Province Development and Reform Commission, China (Grant Number: 2019C036-3). The authors would also like to thank the anonymous reviewers for their helpful comments.

Compliance with Ethical Standards

Conflict of interest The authors declare that they have no conflict of interest.

References

1. Ahmadi, K. (2017). Finite strip modeling of the varying dynamics of thin-walled pocket structures during machining. *The International Journal of Advanced Manufacturing Technology, 89*(9–12), 2691–2699.
2. Li, Y., Daniel, W. J. T., & Meehan, P. A. (2017). Deformation analysis in single-point incremental forming through finite element simulation. *The International Journal of Advanced Manufacturing Technology, 88*(1–4), 255–267.
3. Ye, B., Xiao, W., Mao, K., et al. (2017). Hybrid analytic-experimental modeling for machine tool structural dynamics. *The International Journal of Advanced Manufacturing Technology, 90*(5–8), 1679–1691.
4. Qu, S., Zhao, J., & Wang, T. (2017). Experimental study and machining parameter optimization in milling thin-walled plates based on NSGA-II. *The International Journal of Advanced Manufacturing Technology, 89*(5–8), 2399–2409.
5. Torabi, S. H. R., Alibabaei, S., Barooghi Bonab, B., et al. (2017). Design and optimization of turbine blade preform forging using RSM and NSGA II. *Journal of Intelligent Manufacturing, 28*(6), 1409–1419.
6. Zhang, C., Li, W., Jiang, P., et al. (2017). Experimental investigation and multi-objective optimization approach for low-carbon milling operation of aluminum. *Proceedings of the Institution of Mechanical Engineers, 231*(15), 2753–2772.
7. Yang, S.-H., Lee, H.-H., & Lee, K.-I. I. (2019). Identification of inherent position-independent geometric errors for three-axis machine tools using a double ballbar with an extension fixture. *The International Journal of Advanced Manufacturing Technology, 102*(9–12), 2967–2976.
8. Cai, K., & Wang, D. (2017). Optimizing the design of automotive S-rail using grey relational analysis coupled with grey entropy measurement to improve crashworthiness. *Structural and Multidisciplinary Optimization, 56*(6), 1539–1553.
9. Cao, W. D., Yan, C. P., Wu, D. J., & Tuo, J. B. (2017). A novel multi-objective optimization approach of machining parameters with small sample problem in gear hobbing. *The International Journal of Advanced Manufacturing Technology, 93*(9–12), 4099–4110.
10. Cui, K., & Qin, X. (2018). Virtual reality research of the dynamic characteristics of soft soil under metro vibration loads based on BP neural networks. *Neural Computing and Applications, 29*, 1233–1242.
11. Ma, Y., Tan, J., Wang, D., et al. (2018). Light-weight design method for force performance structure of complex structural part based co-operative optimization. *Chinese Journal of Mechanical Engineering, 31*(1), 1–9.
12. Makaremi, Y., Haghighi, A., & Ghafouri, H. R. (2017). Optimization of pump scheduling program in water supply systems using a self-adaptive NSGA-II; A review of theory to real application. *Water Resources Management, 31*(4), 1283–1304.

13. Zhou, M., Kong, L., Xie, L., et al. (2017). Design and optimization of non-circular mortar nozzles using finite volume method and Taguchi method. *The International Journal of Advanced Manufacturing Technology, 90*(9–12), 3543–3553.
14. Cheng, Q., Zhao, H., Zhao, Y., et al. (2016). Machining accuracy reliability analysis of multi-axis machine tool based on Monte Carlo simulation. *The International Journal of Advanced Manufacturing Technology, 84*(9–12), 2301–2318.
15. Ghasemian, E., & Ehyaei, M. A. (2018). Evaluation and optimization of organic Rankine cycle (ORC) with algorithms NSGA-II, MOPSO, and MOEA for eight coolant fluids. *International Journal of Energy and Environmental Engineering, 9*(1), 39–57.
16. Guo, S., Jiang, G., & Mei, X. (2017). Investigation of sensitivity analysis and compensation parameter optimization of geometric error for five-axis machine tool. *The International Journal of Advanced Manufacturing Technology, 93*(9–12), 3229–3243.
17. Khodaygan, S. (March 2019). An interactive method for computer-aided optimal process tolerance design based on automated decision making. *International Journal on Interactive Design and Manufacturing, 13*(1), 349–364.
18. Lin, C. (2012). Simultaneous optimal design of parameters and tolerance of bearing locations for high-speed machine tools using a genetic algorithm and Monte Carlo simulation method. *International Journal of Precision Engineering and Manufacturing, 13*(11), 1983–1988.
19. Alami Mchichi, N., & Mayer, J. R. R. (2019). Optimal calibration strategy for a five-axis machine tool accuracy improvement using the D-optimal approach. *The International Journal of Advanced Manufacturing Technology, 103*(1–4), 251–265.
20. Sun, L., Ren, M., Hong, H., et al. (2017). Thermal error reduction based on thermodynamics structure optimization method for an ultra-precision machine tool. *The International Journal of Advanced Manufacturing Technology, 88*(5–8), 1267–1277.
21. Tian, M., Gong, X., Yin, L., et al. (2017). Multi-objective optimization of injection molding process parameters in two stages for multiple mass characteristics and energy efficiency using Taguchi method and NSGA-II. *The International Journal of Advanced Manufacturing Technology, 89*(1–4), 241–254.
22. Khoualdia, T., Hadjadj, A. E., Bouacha, K., et al. (2017). Multi-objective optimization of ANN fault diagnosis model for rotating machinery using grey rational analysis in Taguchi method. *The International Journal of Advanced Manufacturing Technology, 89*(9–12), 3009–3020.
23. Ma, C., Zhao, L., Mei, X., Shi, H., et al. (2017). Thermal error compensation of high-speed spindle system based on a modified BP neural network. *The International Journal of Advanced Manufacturing Technology, 89*(9–12), 3071–3085.
24. Xie, Y., Tang, W., Zhang, F., et al. (2019). Optimization of variable blank holder force based on a sharing niching RBF neural network and an improved NSGA-II algorithm. *International Journal of Precision Engineering and Manufacturing, 20*, 285–299.
25. Wang, J., Niu, W., Ma, Y., et al. (2017). A CAD/CAE-integrated structural design framework for machine tools. *The International Journal of Advanced Manufacturing Technology, 91*(1–4), 545–568.
26. Xu, W., & Cao, L. (2019). Optimal maintenance control of machine tools for energy efficient manufacturing. *The International Journal of Advanced Manufacturing Technology, 104*(9–12), 3303–3311.
27. Shen, L., Ding, X., Li, T., et al. (2019). Structural dynamic design optimization and experimental verification of a machine tool. *The International Journal of Advanced Manufacturing Technology, 104*(2), 3773–3786. https://doi.org/10.1007/s00170-019-04049-7.
28. Liu, S., Du, Y., & Lin, M. (2019). Study on lightweight structural optimization design system for gantry machine tool. *Concurrent Engineering, 27*(1), 1063293X1983294. https://doi.org/10.1177/1063293x19832940.
29. Feng, C., & Huang, S. (2020). The analysis of key technologies for sustainable machine tools design. *Applied Sciences, 10*, 731. https://doi.org/10.3390/app10030731.
30. Baptista, A. J., Peixoto, D., Ferreira, A. D., Pereira, J. P., et al. (2018). Lean design-for-X methodology: Integrating modular design, structural optimization and ecodesign in a machine tool case study. *Procedia CIRP, 69*, 722–727.
31. Yuksel, E., Erturk, A. S., & Budak, E. (2020). A hybrid contact implementation framework for finite element analysis and topology optimization of machine tools. *The Journal of Manufacturing Science and Engineering, 142*(8), 081001.

Xueguang Li received the Ph.D. degree in mechanical engineering from Changchun University of Science and Technology, Changchun, China, in 2012. He is an associate professor with the Department of Mechanical Manufacturing and Automation, and the Vice Dean of the College of Mechanical and Electrical Engineering. His research interests include digital design and manufacturing technology, precision and ultra-precision machining technology, NC machining and technics.

Chongqing Li received the B.S. degree in mechanical design, manufacturing and automation from Shenyang Ligong University, Shenyang, China, in 2017, and the M.S. degree in mechanical engineering from Changchun University of Science and Technology, Changchun, Cina, in 2020. His research interests include structural analysis and optimization.

Penghui Li received the bachelor's degree in mechanical engineering from Jilin Agricultural University, Changchun, China, in 2019. He is currently studying for a master's degree in mechanical engineering in Changchun University of Science and Technology, Changchun, China. His research interests include simulation and human-computer interaction.

Huizhong Hu studied mechanical engineering at Changchun University of Technology in China from 2015 to 2019 and received his bachelor's degree in 2019. He is currently studying toward for a master's degree in mechanical engineering at Changchun University of Science and Technology, Changchun, China. His research interests include intelligent assembly and virtual simulation.

Xiansheng Sui received the B.S. degree from Liaoning University of Science and Technology, China, in 2017. He received the M.S. degree from Changchun University of Science and Technology, Changchun, China, in 2020. Now he works in the Design and Research Institute of University of Science and Technology Beijing, and his research direction is intelligent manufacturing.